

Photocatalytic CO₂ reduction in aqueous media using a silver-loaded conjugated polymer and a Ru(II)-Ru(II) supramolecular photocatalyst

Noritaka Sakakibara^{1,*} , Ewan McQueen² , Reiner Sebastian Sprick^{2,*} , Osamu Ishitani^{3,*} 

¹Department of Chemistry, School of Science, Tokyo Institute of Technology, 2-12-1-NE-2 Ookayama, Meguro, Tokyo 152-8550, Japan

²Department of Pure and Applied Chemistry, University of Strathclyde, Thomas Graham Building, 295 Cathedral Street, Glasgow G1 1XL, United Kingdom

³Department of Chemistry, Graduate School of Advanced Science and Engineering, Hiroshima University, 1-3-1 Kagamiyama, Higashi-Hiroshima, Hiroshima 739-8526, Japan

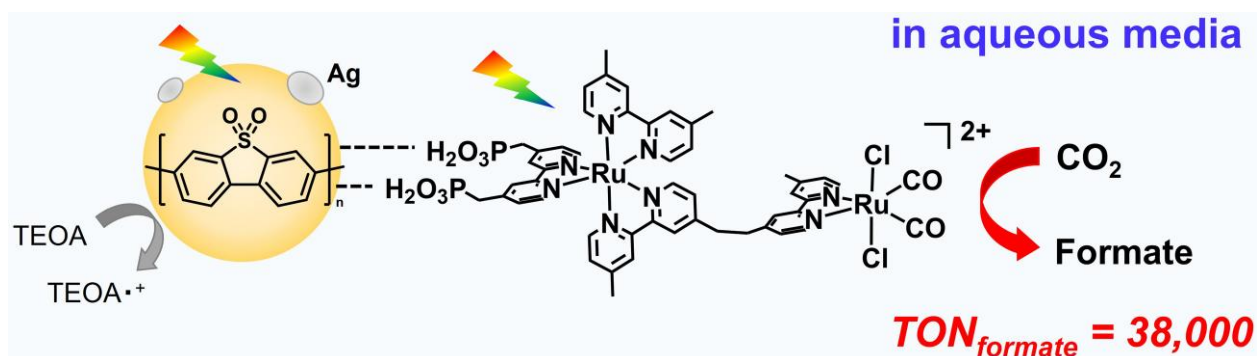
*Corresponding authors: Department of Chemistry, School of Science, Tokyo Institute of Technology, 2-12-1-NE-2 Ookayama, Meguro, Tokyo 152-8550, Japan. Email: nori.sakakibara@gmail.com; Department of Pure and Applied Chemistry, University of Strathclyde, Thomas Graham Building, 295 Cathedral Street, Glasgow G1 1XL, United Kingdom. Email: sebastian.sprick@strath.ac.uk; Department of Chemistry, Graduate School of Advanced Science and Engineering, Hiroshima University, 1-3-1 Kagamiyama, Higashi-Hiroshima, Hiroshima 739-8526, Japan. Email: iosamu@hiroshima-u.ac.jp

Abstract

Visible-light-driven conversion of CO₂ to useful products is a promising process for a more sustainable energy system in a circular economy. Whilst highly efficient, durable, and selective systems have been reported in organic media, the photocatalytic process performing efficiently in aqueous media is highly desirable for the purpose of its practical application. However, efficiency and selectivity for CO₂ reduction versus proton reduction in aqueous solution have proven challenging to date. Herein, this study demonstrates the enablement of highly efficient and durable visible-light-driven photocatalytic CO₂ reduction to formate in aqueous media by a hybrid photocatalyst consisting of a silver-loaded conjugated polymer and a binuclear Ru(II) complex. The hybrid photocatalyst exhibited high activity and durability for formate production, with an apparent quantum yield of 4.2% at 460 nm and a turnover number of 38,000 (based on the amount of binuclear complexes adsorbed), both of which are the highest values reported amongst hybrid photocatalysts in aqueous media. Even though the conjugated polymer retains residual amounts of palladium from synthesis (which is an active site for H₂ production in aqueous media), the loading of Ag nanoparticles onto the conjugated polymer enhanced the activity and selectivity for photocatalytic CO₂ reduction by suppressing H₂ production.

Keywords: CO₂ reduction, conjugated polymer, photocatalyst.

Graphical abstract



[Received on 27 December 2024; revised on 6 February 2025; accepted on 12 February 2025; corrected and typeset on 5 March 2025]

© The Author(s) 2025. Published by Oxford University Press on behalf of the Chemical Society of Japan.

This is an Open Access article distributed under the terms of the Creative Commons Attribution-NonCommercial License (<https://creativecommons.org/licenses/by-nc/4.0/>), which permits non-commercial re-use, distribution, and reproduction in any medium, provided the original work is properly cited. For commercial re-use, please contact reprints@oup.com for reprints and translation rights for reprints. All other permissions can be obtained through our RightsLink service via the Permissions link on the article page on our site—for further information please contact journals.permissions@oup.com.

1. Introduction

The increasing necessity for sustainable energy systems based on carbon-neutral circular models has accelerated research in the field of CO₂ conversion to useful energy-rich products. Among various strategies for CO₂ conversion, photochemical CO₂ reduction is one of the most sustainable approaches because photocatalysts can enable the multielectron reduction of CO₂ to valuable chemicals such as carbon monoxide (CO), formate, and methane by harvesting sunlight as an abundant renewable energy source. Until now, metal complexes,^{1–5} semiconductors,⁶ and their hybrid photocatalysts^{7–9} have been developed for application in solar-driven CO₂ utilization. Among CO₂ reduction products, formic acid has great potential as a liquid carrier of hydrogen gas (H₂) to be used as an alternative energy source to fossil fuels.¹⁰ Since H₂ can be extracted from formic acid using dehydrogenation catalysts,^{11,12} the development of photocatalysts producing formate from CO₂ (which can be easily transformed to formic acid by acidification) has significant potential to contribute to a carbon-neutral energy cycle in the future.

To construct an efficient and durable photocatalytic system for CO₂ reduction using visible light, hybrid photocatalysts are an effective strategy combining semiconductors with adsorbed supramolecular photocatalysts.^{7,8,13–16} Supramolecular photocatalysts consist of two metal complexes bonded directly by a bridging ligand, where one complex acts as a photosensitizer unit for harvesting light energy and the other complex acts as a catalytically active unit for CO₂ conversion.³ For example, the binuclear ruthenium(II) complex (**RuRu'** in **Chart 1**) is a visible-light-responsive supramolecular photocatalyst that has been reported to reduce CO₂ to formate with relatively high durability (turnover number [TON] > 3,000) and high product selectivity (>90%) in organic solutions with a strong reductant, i.e. 1,3-dimethyl-2-phenyl-2,3-dihydro-1*H*-benzo[*d*]imidazole (BIH).^{17,18} The strong reductant is needed to reductively quench the excited state of the photosensitizer due to its low oxidation power as a single component. However, in a hybrid photocatalytic system, a semiconductor capable of absorbing light is introduced, and complexes such as **RuRu'** are adsorbed onto the surface. In this hybrid template, the semiconductor and the photosensitizer unit of the supramolecular photocatalyst allow the step-by-step photoexcitation of both visible-light-responsive components, whilst importantly also enabling more oxidation power in the system, enabling the use of weaker reductants (and most desirably of all the

thermodynamically challenging oxidation of water). This framework is a so-called Z-scheme-type photoexcitation (which mimics natural photosynthesis), and the catalyst unit at the end of the electron cascade ensures selective CO₂ reduction.

In recent years, conjugated polymer semiconductors have emerged as promising visible-light-active photocatalysts for solar-driven fuel production due to their tunable optoelectronic properties and extensive substrate scope through the choice of functional groups in the building blocks.^{19–23} This degree of modularity is very useful in the context of solar light harvesting, which is often limiting for many inorganic semiconductors and graphitic carbon nitride.

Recently, we have developed hybrid photocatalysts for visible-light-driven CO₂ conversion to formate using a series of silver-loaded conjugated polymers and **RuRu'** dispersed in organic solvent, i.e. *N,N'*-dimethylacetamide (DMA) and triethanolamine (TEOA) as a sacrificial reagent.²⁴ The hybrid photocatalyst using the homopolymer poly(dibenzo[*b,d*]thiophene sulfone), P10 as shown in **Chart 1**, i.e. **RuRu'**/Ag/P10, demonstrated very efficient and durable formate production (Scheme 1). P10 has been previously reported showing very high activity for photocatalytic hydrogen production^{23,25} from water under sacrificial conditions and has even been reported to achieve overall water splitting when loaded with metal cocatalysts.²⁶ In the case of the hybrid photocatalyst **RuRu'**/Ag/P10 for CO₂ reduction, the system displayed a very high TON of 349,000 and an apparent quantum yield (AQY) of 11.2% at 440 nm for formate production. Remarkably, this activity enabled quantitative conversion of CO₂ to formate under standard temperature and pressure, hence also enabling the formation of very high concentrations of formate up to a concentration of 0.4 M by periodical replenishment of the CO₂ feedstock. Whilst these high concentrations of formate enabled by visible-light-driven conversion are certainly appealing for future practical application, the photocatalytic process was performed in an entirely organic medium.

Going forward, the process proceeding in aqueous media is highly desirable as it is easier to handle, and to date, various types of such systems have been developed.^{15,27–44} Furthermore, developing the photocatalytic CO₂ reduction system in aqueous media is essential to target truly artificial photosynthetic systems where water molecules themselves are the electron donor, thus producing systems that generate energy rather than facilitating energetically downhill reactions.^{6,45} However, problematic issues in performance can arise because of the proton-rich environment in aqueous media, incurring a competitive reduction pathway for

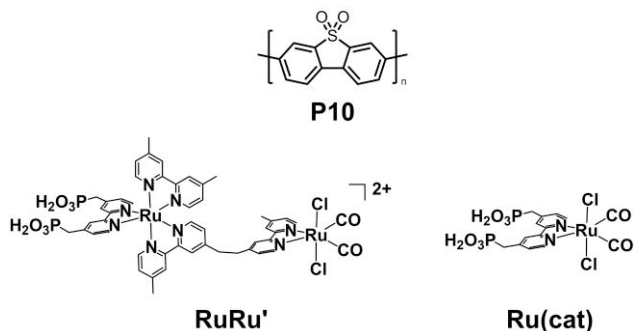
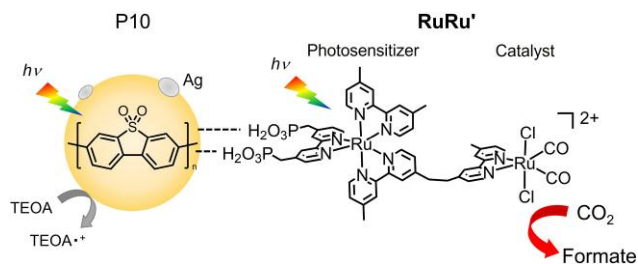


Chart 1. Structures and abbreviations of the conjugated polymer, supramolecular photocatalyst, and metal complex used in this study.



Scheme 1. Illustration of CO₂ reduction by the hybrid photocatalyst (**RuRu'**/Ag/P10) under visible light irradiation.

photogenerated electrons producing hydrogen gas (which otherwise could be used to increase the yield of CO₂ reduction products). This selectivity can be particularly problematic when using conjugated polymers in aqueous media because of the residual palladium that remains in the material from synthesis, which can act as efficient active sites for proton reduction.^{46–49} Thus, strategies to use these highly active polymer photocatalysts for processes other than proton reduction are highly sought after but to date remain challenging.

Herein, we investigated the photocatalytic CO₂ reduction capability of the hybrid photocatalyst **RuRu'**/Ag/P10 in aqueous media. In an aqueous solution containing acetonitrile (MeCN) and TEOA (H₂O:MeCN:TEOA = 3:1:1, v/v) containing 20 mM Na₂CO₃, the hybrid photocatalyst produced formate efficiently with an AQY of 4.2%. The silver (Ag) loading onto P10 improved the activity and selectivity of photocatalytic CO₂ reduction by suppressing H₂ production occurring on the residual Pd in P10. This effect of Ag loading was also supported by light-induced electron spin resonance (ESR) measurements. The TON for formate production (based on the amount of **RuRu'** used) was 38,000 after 48 h of visible light irradiation, which is the highest durability reported among hybrid photocatalysts comprising of semiconductors and metal complexes for CO₂ reduction in aqueous media.

2. Experimental

2.1 Materials

MeCN and TEOA were distilled, and H₂O was deionized before use. ¹³CO₂ (99% ¹³C isotope) was purchased from Cambridge Isotope Laboratories, Inc. All other reagents were commercially available and used without further purification.

2.2 Preparation of hybrid photocatalysts

Ru complexes (**RuRu'** and **Ru(cat)**) were prepared using previously reported methods.^{3,50,51} Conjugated polymer P10 was prepared by Pd(0)-catalyzed Suzuki–Miyaura polycondensation.^{23,24} In a 100 mL 2-necked flask, 3,7-dibromodibenzo[*b,d*]thiophene sulfone (561.9 mg, 1.5 mmol) and 3,7-bis(4,4,5,5-tetramethyl-1,3,2-dioxaborolan-2-yl)dibenzo[*b,d*]thiophene sulfone (702 mg, 1.5 mmol) tetrakis(triphenylphosphine)palladium(0) (5.19 mg, 0.3 mol%) and potassium carbonate (1036.5 mg, 7.5 mmol) were added with a stirring bar. The reagents were evacuated under vacuum and purged with argon in 3 cycles. Degassed *N,N'*-dimethylformamide (30 mL) and degassed water (7.5 mL) were added, and the mixture was refluxed at 150 °C under nitrogen for 3 days with continuous stirring. The solid powders were collected, washed with water and methanol, and further purified by Soxhlet extraction with chloroform overnight to remove low-molecular-weight by-products. A yellow powder was obtained as a solid product (615 mg, 95%). Ag was loaded at 1 wt% onto P10 by an impregnation method using AgNO₃ (>99.8%, Wako Pure Chemicals Co.) as a precursor with subsequent heating under a H₂ stream (20 mL min⁻¹) at 473 K for 1 h.²⁴ For the preparation of hybrid photocatalyst **RuRu'**/Ag/P10, **RuRu'** was loaded onto the Ag-loaded P10 by dispersing in an MeCN solution of **RuRu'**, and the suspension was stirred in the dark at

room temperature overnight. The obtained powder was collected via filtration, washed with MeCN, and dried under reduced pressure.

2.3 Characterization

Diffuse reflectance spectra were obtained using a V-770 (JASCO) spectrometer equipped with an integration sphere using a Spectralon reference standard (6916-H422A, JASCO) as a reference. Fourier transform infrared (FT-IR) spectroscopy of powder samples were performed using FT/IR-6600 (JEOL) in a diffuse reflectance configuration. UV-Vis absorption spectroscopy of solutions was performed using a V-700 (Jasco) spectrometer. X-ray photoelectron spectroscopy (XPS) was conducted using ESCA-3400 (Shimadzu). The binding energy values were corrected using that of C 1s peak (285 eV) as an internal reference, which is the signal from hydrocarbon contamination. Inductively coupled plasma–optical emission spectroscopy (ICP-OES) was performed using 5100 VDV ICP-OES (Agilent Technologies) to quantify Ru (ions) on the hybrid photocatalyst. Ten milliliters of nitric acid and 10 mg of the hybrid photocatalyst were used to prepare the sample for ICP-OES.

2.4 Photocatalytic CO₂ reduction

To an 8-mL test tube, the hybrid photocatalysts were dispersed in 4 mL of an aqueous solution consisting of H₂O, MeCN and TEOA (3:1:1, v/v), also with 20 mM of sodium carbonate (Na₂CO₃). Prior to irradiation, the suspension was purged by bubbling CO₂ for 30 min. Visible light from a 460 nm-centered LED light source was used with continuous stirring of the reaction vessel enabled by a merry-go-round-type photo-irradiation apparatus, Iris-MG (CELL System Co.). After light irradiation, gaseous products of photocatalysis, i.e. CO and H₂, were analyzed by a gas chromatograph system equipped with a thermal conductivity detector (GC-TCD, GL Science GC323), using an activated carbon column and argon carrier gas. The amount of formate generated in the liquid phase was determined using a capillary electrophoresis system (Agilent Technologies 7100 L).

2.5 AQY measurements

AQY measurements for CO₂ reduction to formate were performed by dispersing the hybrid photocatalyst in 10 mL of H₂O/MeCN/TEOA (3:1:1, v/v) containing 20 mM Na₂CO₃. A 300-W Xe light source (MAX-303, Asahi Spectra) with a 460 nm band-pass filter was used. Monochromatic light with an intensity of 2.8 mW/cm² was sustained for 1 h, resulting in 3.9 × 10⁻⁵ Einstein based on the total number of incident photons. The light intensity was measured using a spectroradiometer (Eko Instruments, LS-100). In the AQY measurement, the adsorption amount of **RuRu'** for the hybrid photocatalyst was 10 μmol g⁻¹.

In this study, AQY was calculated using the basic definition of quantum yield⁴ which is as follows:

$$\text{AQY}(\%) = \frac{\text{(total amount of formate produced)}}{\text{(total number of incident photons)} \times 100}. \quad (1)$$

In many previous reports in the literature, “AQY” is given the coefficient “2” because 2 electrons are necessary to produce 1 CO₂ reduction product such as CO and formate. However, the reaction mechanism of the hybrid system is very

complicated and has not been fully elucidated yet. As such, we tentatively do not use the definition of AQY with a coefficient of 2, especially when highly reactive 1-electron oxidized species, as well as Z-scheme and direct electron pathways both being thermodynamically permissible, infer that the accounting of photons to electrons in a 1:1 ratio cannot be assumed with confidence.

2.6 Isotope tracer experiment

Isotopically labeled CO_2 ($^{13}\text{CO}_2$) gas was introduced into a glass reactor filled with 2 mL of $\text{H}_2\text{O}/\text{MeCN}/\text{TEOA}$ (3:1:1, v/v) containing 20 mM of isotopically labeled sodium carbonate ($\text{Na}_2^{13}\text{CO}_3$) and 4 mg of the hybrid photocatalyst powder after the aqueous dispersion underwent freeze-pump-thaw degassing 3 times. The ^1H NMR spectrum of the reaction solution after 65 h of irradiation with a 460 nm-centered LED was measured by a JNM-ECA 400 spectrometer (JEOL) at 400 MHz using the no-deuterium proton technique. The solids were removed by filtration before the measurement.

2.7 ESR spectroscopy

ESR spectroscopy of P10 and Ag-loaded P10 powders were performed using the EMXplus (Bruker) at the Institute for Molecular Science. The sample powders were placed in a quartz tube, evacuated under vacuum and purged with nitrogen in 3 cycles, and filled with nitrogen gas for measurements and sealed. The measurements were performed at room temperature using microwaves in the X-band range (9.6 GHz) at 1.002 mW. The center of the magnetic field was set to 3524.8 G, with a sweep width of 200 G. The receiver gain, modulation amplitude, and microwave attenuation were set to 30 dB, 0.5 G, and 23 dB, respectively. The scan number and modulation frequency were set to 20 and 100 kHz, respectively. The g -value was calibrated by a sharp peak of 2,2-diphenyl-1-picrylhydrazyl (DPPH, $g = 2.0036$) before the measurement. A Hg–Xe lamp (SLS400, Thorlabs) was used to obtain ESR spectra under light irradiation with a cold filter (CLDF-50S, Sigmakoki) for UV–vis light irradiation (750 nm $>$ λ_{ex} $>$ 360 nm) and a red dichroic filter (DIF-50S-RED, Sigmakoki) for red light irradiation (λ_{ex} $>$ 550 nm). The output powers of the lamp through the filters were 124 and 95 mW for the UV–vis and red light, respectively.

3. Results and discussion

P10,²³ RuRu' ,³ and the hybrid photocatalyst ($\text{RuRu}'/\text{Ag}/\text{P10}$)²⁴ were all prepared as reported in our previous studies. For the preparation of the hybrid photocatalysts, 1 wt. % of silver nanoparticles were loaded onto P10, as it has been reported that the Ag loading improves charge separation of photoexcited carriers in organic semiconductor materials^{14,52} including P10.²⁴ Ag nanoparticles smaller than 50 nm covered the whole surface of P10, as evidenced by STEM/EDS in our previous study.²⁴ Subsequently, RuRu' was adsorbed onto the silver-loaded P10 (Ag/P10) by dispersing in a MeCN solution containing RuRu' overnight in the dark to obtain the hybrid photocatalyst. The incorporation of RuRu' onto the hybrid photocatalyst was identified by the appearance of vibration peaks of the carbonyl ligands of the Ru catalyst unit in the FT-IR spectrum (Supplementary Fig. S1).

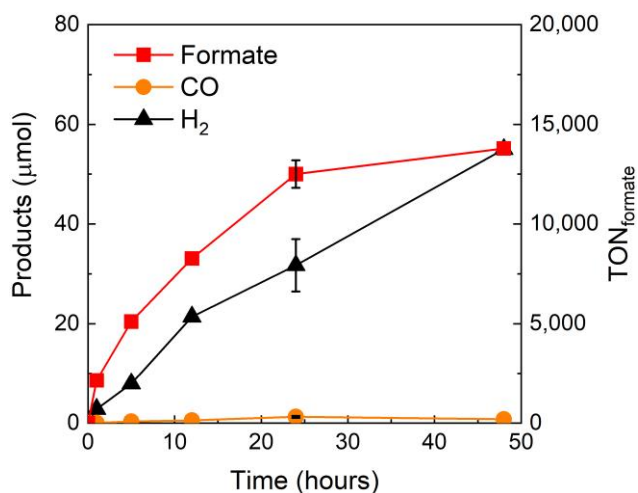


Fig. 1. Product formation over time and corresponding $\text{TON}_{\text{formate}}$ during light irradiation with 4 mg of $\text{RuRu}'/\text{Ag}/\text{P10}$ in 4 mL of $\text{H}_2\text{O}/\text{MeCN}/\text{TEOA}$ (3:1:1, v/v) containing 20 mM Na_2CO_3 under CO_2 atmosphere. The loading amount of RuRu' was $1 \mu\text{mol g}^{-1}$.

As a typical photocatalytic reaction, the hybrid photocatalyst was dispersed in a mixed solution of H_2O , MeCN, and TEOA (3:1:1, v/v) containing 20 mM Na_2CO_3 with stirring under a CO_2 atmosphere and irradiated using an LED light source with a center wavelength at 460 nm. Na_2CO_3 was added to obtain basic conditions since it has been previously reported that formate formation by the Ru(II) catalyst is favorable under basic conditions.² The LED light simultaneously allows the optical-gap excitation of P10 and the $^1\text{MLCT}$ excitation of the photosensitizer unit of RuRu' (Supplementary Fig. S2). Fig. 1 shows the product formation over time during the irradiation using $\text{RuRu}'/\text{Ag}/\text{P10}$ with $1 \mu\text{mol g}^{-1}$ of RuRu' loading. After 1 h of irradiation, formate was produced as the primary product (8.6 μmol) with H_2 (2.8 μmol) and CO (0.07 μmol) as minor products. The product selectivity was 75% for formate production. The yield corresponds to a turnover frequency ($\text{TOF}_{\text{formate}}$) of 2150 h^{-1} based on the amount of RuRu' used. The yield of formate increased according to the irradiation time, and 56 μmol of formate ($\text{TON}_{\text{formate}}$ of 13,800) was produced with 50% selectivity after 48 h of irradiation.

The carbon source of the produced formate was identified through a $^{13}\text{CO}_2$ isotopic labeling experiment. As shown in Fig. 2, a doublet attributed to an equilibrium mixture of H^{13}COOH and $\text{H}^{13}\text{COO}^-$ was observed at $\delta = 8.4 \text{ ppm}$ with $J = 192 \text{ Hz}$ (red), while a very small singlet attributable to that of H^{12}COOH and $\text{H}^{12}\text{COO}^-$ was detected. Conversely, only a singlet was observed at 8.4 ppm (black) for the photocatalytic reaction under an ordinary CO_2 atmosphere, thereby confirming formate was produced from CO_2 .

The chemical stability of P10 and Ag during the photocatalytic reaction was indicated by FT-IR spectroscopy and XPS spectra at S-2p and Ag-3d regions, which showed no change in the spectra after the irradiation (Supplementary Figs. S3 and S4). However, the desorption of RuRu' from the hybrid photocatalyst after irradiation was evaluated to be 63.5% by an ICP-OES measurement. This strongly suggests that the main reason for the performance degradation of the hybrid system is the desorption of RuRu' during photocatalysis. In fact, when the hybrid photocatalyst was stirred in $\text{H}_2\text{O}/$

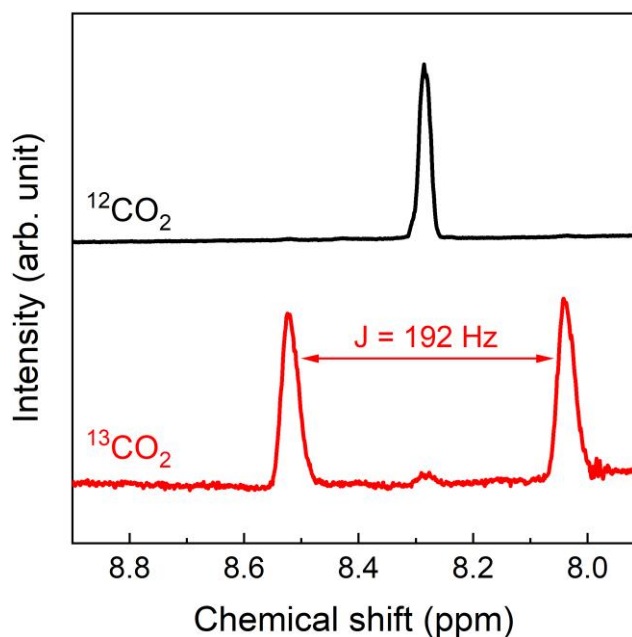


Fig. 2. ^1H NMR spectra of the $\text{H}_2\text{O}/\text{MeCN}/\text{TEOA}$ (3:1:1, v/v) aqueous solution containing 20 mM $\text{Na}_2^{13}\text{CO}_3$ after photocatalysis using $\text{RuRu}'/\text{Ag}/\text{P10}$. For the photocatalysis, the suspension of $\text{RuRu}'/\text{Ag}/\text{P10}$ was irradiated by a 460 nm LED for 65 h under $^{13}\text{CO}_2$ and unlabeled CO_2 .

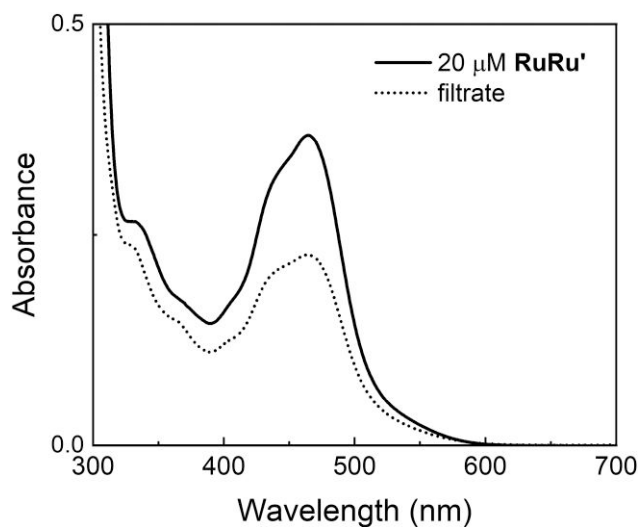


Fig. 3. UV-vis absorption spectrum of the filtrate solution after stirring $\text{RuRu}'/\text{Ag}/\text{P10}$ ($1 \mu\text{mol g}^{-1}$ of RuRu' loading) for 3 d in the dark (dotted line). UV-vis absorption spectrum of 20 μM RuRu' (black line), which corresponds to the RuRu' concentration if hypothetically all of the RuRu' was desorbed from the hybrid photocatalyst. The spectra indicated 61.5% desorption of RuRu' from the hybrid photocatalyst.

MeCN/TEOA (3:1:1, v/v) containing 20 mM Na_2CO_3 for 3 d in the dark, 61.5% of RuRu' was found to have desorbed as quantified by the UV-vis absorption spectrum of the filtrate solution (Fig. 3). Quantification was performed by calculating the ratio of the $^1\text{MLCT}$ absorption of the photosensitizer unit of RuRu' in the filtrate to that of 20 μM RuRu' (which corresponds to the amount of RuRu' if all that had been incorporated in the hybrid photocatalyst had desorbed in theory).

By contrast, this degree of desorption was not observed in DMA/TEOA (4:1, v/v) in our previous study of the hybrid system.²⁴ Thus, the desorption can be attributed to the lower stability of the interaction between the polymer P10 and RuRu' in aqueous media. Nevertheless, it should be pointed out that the $\text{TON}_{\text{formate}}$ was notably large (in excess of 10,000, Fig. 1) using this aqueous solution.

The effects of MeCN and different electron donors were tested by comparing the results of photocatalysis using $\text{RuRu}'/\text{Ag}/\text{P10}$ after 5 h of irradiation (Table 1). When the photocatalytic experiment was conducted in the absence of MeCN, i.e. in a $\text{H}_2\text{O}/\text{TEOA}$ (4:1, v/v) mixed solution containing 20 mM Na_2CO_3 (entry 2), the yield of formate decreased by 2.9 times whilst the H_2 yield increased by 1.8 times compared with the presence of MeCN (entry 1), leading to lower $\text{TON}_{\text{formate}}$ and selectivity for formate production. We presumed two possible advantages of adding MeCN: to improve the dispersibility of P10 in the medium; and to improve the stability of the catalytic CO_2 reduction cycle involving the $\text{Ru}(\text{II})$ catalyst unit through the coordination of MeCN,⁵⁴ although further studies are necessary to confirm this. When using triethylamine (TEA) as an electron donor (entry 3), the yield of formate and its selectivity slightly increased compared with the system using TEOA (entry 1). When using ascorbic acid, on the other hand, the yield of formate drastically decreased (entry 4) even though ascorbic acid has a higher oxidation potential (E_{OX}) compared with TEOA and TEA. When comparing the previous studies of photocatalytic hydrogen production using copolymers incorporating the dibenzo[*b*, *d*]thiophene sulfone unit in the main chain, use of TEA as a sacrificial electron donor demonstrated superior activity for hydrogen production compared with ascorbic acid.^{23,55} The same activity trend is observed in this study. Lastly, CO_2 reduction products (formate and CO) were not observed when using ethylenediaminetetraacetic acid disodium salt dihydrate ($\text{EDTA}\cdot 2\text{Na}$) as an electron donor.

The AQY for photocatalytic CO_2 reduction by the hybrid system was evaluated using the basic definition of quantum yield (Eq. 1).⁴ An AQY of 4.2% was obtained at $\lambda_{\text{ex}} = 460 \text{ nm}$ in a mixed solution of H_2O , MeCN, and TEOA (3:1:1, v/v) containing 20 mM Na_2CO_3 . This AQY value is the highest value among reports of photocatalytic CO_2 reduction using hybrid systems comprising of semiconductors and metal complexes in aqueous media^{15,32,33,38,39} using the conventional definition of quantum yield. Actually, we note that the highest AQY value was reported as 5.1% with a hybrid system under aqueous conditions for CO production.³² That being said, we highlight that this value was calculated using the equation for AQY with a coefficient of 2 to account for the 2-electron reduction of CO_2 , i.e. = 2.6% if using the AQY definition used in this study. As such, we report within reason that the AQY value obtained in this study (4.2%) is the highest value so far.

Table 2 summarizes the results of control experiments in the absence of one or some component(s) of the photocatalytic reaction after 1 h of irradiation. In the absence of CO_2 , i.e. under Ar atmosphere (entry 2), TEOA (entry 3), and light irradiation (entry 4), no CO_2 reduction products (formate and CO) were detected. The homogeneous system using only RuRu' did not produce any reduction products of CO_2 (entry 5), indicating that TEOA does not directly donate an electron to the excited state of the photosensitizer unit of RuRu' , in good agreement with the previous report that the $\text{Ru}(\text{II})$ photosensitizer cannot

Table 1. Photocatalytic CO₂ reduction using the hybrid photocatalyst using different electron donors^a.

Entry	Reductant	E_{OX}^b/V vs SCE	Products/ μmol			TON _{formate}	Selectivity _{formate} /%
			Formate	CO	H ₂		
1	TEOA (w/MeCN) ^c	0.57 to 0.82	20	0.32	7.9	4960	71
2	TEOA	0.57 to 0.82	6.9	0.55	14	1740	32
3	TEA (w/MeCN) ^d	0.69	25	0.24	4.4	6320	84
4	Ascorbic acid (20 mM)	0.46	0.88	0.08	2.9	220	23
5	EDTA·2Na (20 mM)	0.57 to 0.92	ND	ND	0.84	—	—

^aReaction conditions: 4 mg of the hybrid photocatalyst (**RuRu'** loading: 1 $\mu\text{mol g}^{-1}$; Ag loading: 1 wt%); 4.0 mL of solutions containing 20 mM Na₂CO₃ bubbled with CO₂; irradiation time: 5 h.

^bValues of oxidation potentials (E_{OX}) are taken from a review article.⁵³

^cH₂O/MeCN/TEOA (3:1:1, v/v).

^dH₂O/MeCN/TEA (3:1:1, v/v).

Table 2. Photocatalytic CO₂ reduction and control experiment results^a.

Entry	Photocatalyst	Absence	Products/ μmol			TOF/h ⁻¹	Selectivity _{formate} /%
			Formate	CO	H ₂		
1	RuRu' /Ag/P10	—	14.3	0.07	1.34	3570	91
2	RuRu' /Ag/P10	CO ₂	ND	ND	14.7	—	—
3	RuRu' /Ag/P10	TEOA	ND	ND	ND	—	—
4	RuRu' /Ag/P10	Light	ND	ND	ND	—	—
5	RuRu'	Ag/P10	ND	ND	ND	—	—
6	P10	RuRu' and Ag	ND	ND	9.79	—	—
7	Ag/P10	RuRu'	ND	0.25	11.2	—	—
8	RuRu' /P10	Ag	0.69	0.33	10.9	170	5.8
9	Ru(cac) /Ag/P10	—	3.33	ND	4.54	830	42

^aReaction conditions: 4 mg of photocatalyst (loadings of metal complexes: 1 $\mu\text{mol g}^{-1}$; Ag loading: 1 wt%); 4.0 mL of H₂O/MeCN/TEOA (3:1:1, v/v) containing 20 mM Na₂CO₃ bubbled with CO₂; Irradiation time: 1 h.

be quenched by TEOA.⁵⁶ P10 (entry 6) and Ag/P10 (entry 7) without adsorption of **RuRu'** also did not produce any CO₂ reduction product, highlighting the importance of the hybrid construct for photocatalytic CO₂ reduction.

The hybrid photocatalyst without Ag loading (**RuRu'**/P10, entry 8) produced much lower formate (0.69 μmol) compared with **RuRu'**/Ag/P10 (14.3 μmol , entry 1) while the yield of H₂ was much higher (10.9 μmol) than that of **RuRu'**/Ag/P10 (1.34 μmol). This result clearly shows that Ag loading onto P10 is advantageous to gain the high photocatalytic CO₂ reduction activity and selectivity using the hybrid system compared with hydrogen evolution. From synthesis, residual amounts of palladium (Pd) reside on the P10 material (70 ppm were determined²⁴). Palladium is known to be an active catalyst for proton reduction to form H₂ thereby hampering selectivity for CO₂ reduction.^{46–49} Nevertheless, the hydrogen overpotential using Ag is much larger than that of Pd,⁵⁷ so we hypothesize that the Ag particles suppress H₂ evolution as well as efficiently pass electrons to **RuRu'**, as correlated with the observed photocatalytic activity with and without silver. Although our previous report of the P10 hybrid system in a nonaqueous medium suggested that Ag loading onto different semiconducting materials other than conjugated polymers improved charge separation of photoexcited carriers,^{14,52} such effects were not as obvious in the present hybrid system in aqueous media. This is particularly obvious when considering the total yield of reduction products (formate, CO and H₂) produced by the hybrid photocatalyst with Ag loading (15.7 μmol , entry 1) was similar to that without Ag loading (11.9 μmol , entry 1), whereas, in DMA/TEOA (4:1, v/v), a factor of 3.6 increase in the amount of the reduction products was observed with Ag loading.²⁴ Hence, it is

interesting to observe the dependence of Ag behavior on the reaction medium, particularly in the case of aqueous media, where a remarkable increase in selectivity for CO₂ reduction is observed relative to proton reduction. This is a notable observation considering the high concentration of protons in an aqueous environment.

ESR spectroscopy of P10 and Ag/P10 was performed in the X-band region to further investigate the role of the Ag loading onto P10. In the dark, both P10 and Ag/P10 demonstrated single peaks at $g = 2.0041$ and 2.0045 , respectively (Fig. 4a and b), which could be attributed to defects involving unpaired electrons in π conjugation.^{58,59} Under irradiation with UV-vis light ($750 \text{ nm} > \lambda_{\text{ex}} > 360 \text{ nm}$), the signal intensity of the peak in both P10 and Ag/P10 was enhanced, accompanied with a new sharp peak prominent in the P10 spectrum (Fig. 4a and b). The difference in spectra between illumination and dark conditions, i.e. light-induced ESR spectra (LESR), are shown in Fig. 4c and d. Since the red light ($\lambda_{\text{ex}} > 550 \text{ nm}$) irradiation decreased the light-induced change in the spectra (Supplementary Fig. S5) and the ESR spectra recovered to the original spectra after the UV-vis and red light irradiation (Supplementary Fig. S6), the LESR signals are attributed to the photoexcitation of P10 and Ag/P10. The spectra were deconstructed into 2 peaks (Fig. 4c and d, Table 3): one is the sharp peak at $g = 2.0027$ with a peak width (ΔH_{pp}) of 2.24 G for P10 and $g = 2.0027$ with ΔH_{pp} of 2.27 G for Ag/P10 (noted as comp A); and the other is the broad peak at $g = 2.0040$ with ΔH_{pp} of 11.4 for P10 and at $g = 2.0044$ with ΔH_{pp} of 10.1 for Ag/P10 (comp B). Since the g values of comp B were similar to those of ESR signals in the dark, comp B can be attributed to the accumulation of photoexcited electrons in π conjugation.¹⁶ The intensity of comp B is slightly

higher in Ag/P10 than in P10, suggesting that there is a slight enhancement in photoexcited charge accumulation in the polymer by the Ag loading, probably owing to the improved charge separation.⁵² The higher intensity of comp B by Ag loading was also observed for a carbon nitride in our previous study.⁵² On the other hand, the intensity of comp A is 3.6 times higher in P10 than in Ag/P10. It was previously reported that Pd-loaded TiO₂ shows a strong sharp peak at $g = 2.0016$ – 2.0024 under light irradiation from a photoexcited hole at the Pd/TiO₂ interface due to the transfer and accumulation of photoexcited electrons to Pd nanoparticles on TiO₂.⁶⁰ In contrast, it was reported that Pd nanoparticles with magic atom number give a sharp ESR signal at $g = 2.00$ due to the one s-state electron outside the closed electron shell.⁶¹ Thus, the

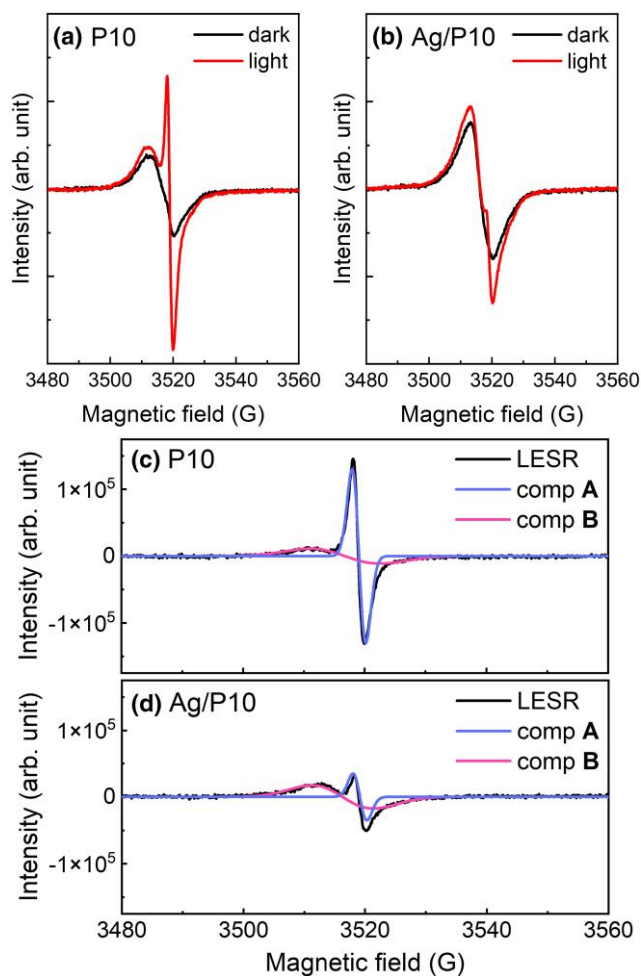
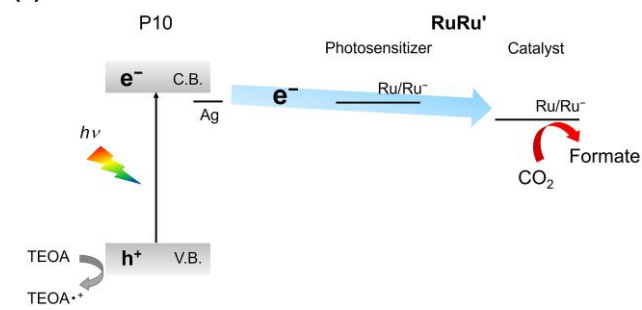


Fig. 4. ESR spectra in the dark and under UV-vis light ($750 \text{ nm} > \lambda_{\text{ex}} > 360 \text{ nm}$) irradiation of a) P10 and b) Ag/P10. LESR spectra of c) P10 and d) Ag/P10. The LESR spectra were deconstructed into 2 components, i.e. comp A and comp B, by Gaussian fitting. The fitting parameters are listed in Table 3.

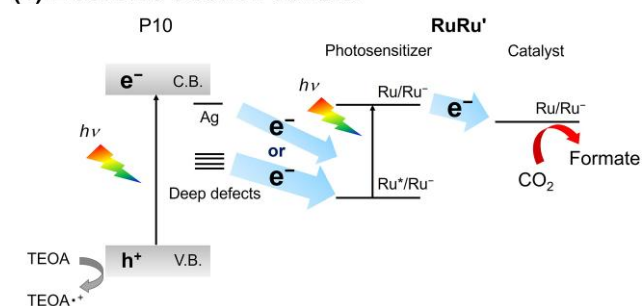
comp A in this study might be related to the photoexcited carriers at the interface between the residual Pd and the conjugated backbone of P10, i.e. accumulation of photoexcited electrons into the residual Pd and resultant hole on P10, although we cannot fully assign the peaks at this stage. Therefore, this light-induced ESR spectroscopy result suggests that Ag loading onto P10 suppresses the accumulation of photoexcited electrons to residual Pd, which is in line with the results observed in the photocatalytic control experiments detailed in Table 2.

When a ruthenium mononuclear catalyst **Ru(cat)**, which is a mononuclear model complex of the catalytic unit of **RuRu'** (Chart 1), was used instead of **RuRu'**, the hybrid photocatalyst (**Ru(cat)/Ag/P10**) was still active for photocatalytic CO₂ reduction (entry 9). However, the production of formate ($3.33 \mu\text{mol}$) decreased compared with that of **RuRu'/Ag/P10** ($14.3 \mu\text{mol}$), whereas the H₂ production increased ($4.54 \mu\text{mol}$) compared with that of **RuRu'/Ag/P10** ($1.34 \mu\text{mol}$), accompanied by lower selectivity (42%) for formate production. This result can be reasonably explained by assuming 2 possible electron transfer pathways from Ag/P10 to the catalyst unit of **RuRu'**: one is a potential direct electron transfer from Ag/P10 to the catalyst unit without photoexcitation of the photosensitizer unit of **RuRu'** (Scheme 2a); and the

(a) Direct electron transfer



(b) Z-scheme electron transfer



Scheme 2. Illustration of the possible electron transfer pathways in the hybrid photocatalyst (**RuRu'/Ag/P10**) under visible light irradiation. a) Direct electron transfer via 1-photon excitation. b) Z-scheme electron transfer via 2-photon excitation.

Table 3. List of fitting parameters of LESR spectra, i.e. center position (H_c), g -value, line width (ΔH_{pp}) and amplitude (Amp) of each component.

Sample	Comp A			Comp B		
	H_c/G (g -value)	$\Delta H_{\text{pp}}/G$	Amp	H_c/G (g -value)	$\Delta H_{\text{pp}}/G$	Amp
P10	3519.09 (2.0027)	2.24	673,354	3516.82 (2.0040)	11.4	1,510,895
Ag/P10	3519.17 (2.0028)	2.27	187,580	3516.31 (2.0044)	10.1	1,841,883

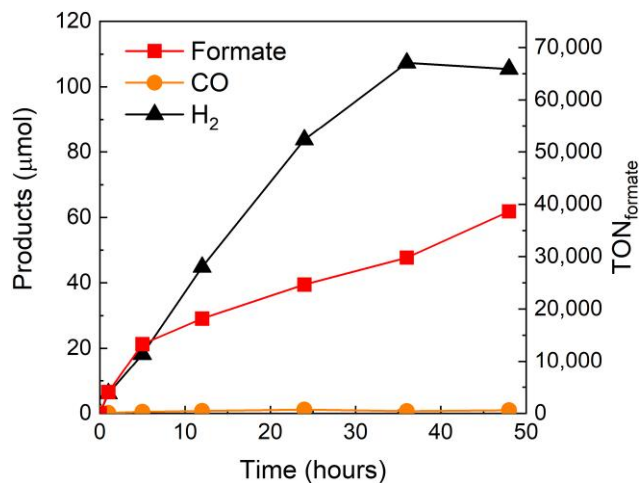


Fig. 5. Product formation over time and corresponding $\text{TON}_{\text{formate}}$ during visible-light irradiation with 4 mg of $\text{RuRu}'/\text{Ag}/\text{P10}$ in 4 mL of $\text{H}_2\text{O}/\text{MeCN}/\text{TEOA}$ (3:1:1, v/v) containing 20 mM Na_2CO_3 under CO_2 atmosphere. The loading amount of RuRu' was $0.4 \mu\text{mol g}^{-1}$.

other potential mechanism is a Z-scheme-type electron transfer *via* step-by-step excitation of both P10 and the photosensitizer unit of RuRu' (Scheme 2b), as reported previously.²⁴ In the system using $\text{Ru}(\text{cat})/\text{Ag}/\text{P10}$, electrons accumulated in deep defect bands of P10, which cannot be transferred to the catalyst unit, may otherwise contribute to H_2 production *via* transfer to Pd centers. In the system using $\text{RuRu}'/\text{Ag}/\text{P10}$, on the other hand, the Z-scheme-type electron transfer potentially enables such electrons in deep defect sites to be re-excited by the photosensitizer unit of RuRu' and finally transfer to the catalyst unit of RuRu' (Scheme 2b).

The durability of the supramolecular photocatalyst RuRu' on $\text{Ag}/\text{P10}$ was further investigated by using a smaller amount of RuRu' to incorporate on the surface of $\text{Ag}/\text{P10}$ ($0.4 \mu\text{mol g}^{-1}$ instead of $1 \mu\text{mol g}^{-1}$ that was used in Fig. 1). The results are shown in Fig. 5: the $\text{TON}_{\text{formate}}$ reached 38,000 after 48 h of irradiation (with 37% selectivity for formate production). This TON is, to the best of our knowledge, the highest value reported among hybrid photocatalysts comprising of semiconductors and metal complexes for CO_2 reduction in aqueous media,^{15,33,38,40} although there is a remarkable preceding report of a homogeneous photocatalytic system that demonstrated CO_2 reduction to CO with TON over 80,000 using quantum dots and a cobalt-porphyrin catalyst.²⁷

4. Conclusion

The hybrid photocatalyst consisting of Ag-loaded P10 and RuRu' ($\text{RuRu}'/\text{Ag}/\text{P10}$) showed highly efficient and durable photocatalytic CO_2 reduction to formate even in an aqueous medium. The AQY of the hybrid system for formate production was 4.2% under 460 nm monochromatic irradiation. The Ag loading onto P10 improved the activity and product selectivity for photocatalytic CO_2 reduction to formate by suppressing H_2 production via residual Pd centers in P10, which was supported by light-induced ESR spectroscopy. After 48 h of irradiation, the hybrid photocatalyst produced formate with a TON of 38,000 (based on the amount of RuRu' loaded). These values are the highest among hybrid photocatalysts for photocatalytic CO_2 reduction in aqueous

media reported so far. We found that the main deactivation process was detachment of RuRu' from the surface of $\text{Ag}/\text{P10}$. These results suggest that reinforcement of the binding between the supramolecular photocatalyst and the surface of $\text{Ag}/\text{P10}$ is required, and this is now being investigated in our laboratory.

Acknowledgments

The authors thank the Open Facility Center, Tokyo Institute of Technology, for ICP-OES measurements. ESR measurements were performed at the Institute for Molecular Science, supported by Nanotechnology Platform Program (JPMXP1223MS1087) of the Ministry of Education, Culture, Sports, Science and Technology (MEXT), Japan.

Supplementary data

FT-IR spectra, diffuse reflectance spectra, spectrum of LED light source, XPS spectra and ESR spectra. [Supplementary material](#) is available at *Bulletin of the Chemical Society of Japan* online.

Funding

N.S. thanks Japan Society for the Promotion of Science (JSPS) (KAKENHI grant numbers: JP21J01295, JP23K13821). O.I. thanks JSPS (KAKENHI grant numbers: JP20H00396, JP17H06440) and the Iwatani Naoji Foundation for their financial support. R.S.S. thanks University of Strathclyde for financial support through The Strathclyde Chancellor's Fellowship Scheme and Royal Society grant for an International Exchanges (IES\R2\212040). E.M. thanks EPSRC for funding through a Doctoral Training Partnership postgraduate studentship (EP/T517938/1).

Conflict of interest statement. None declared.

Data availability

The data underlying this article are available in the article and in its online [Supplementary material](#).

References

- J. Hawecker, J.-M. Lehn, R. Ziessel, *Helv. Chim. Acta* **1986**, *69*, 1990. <https://doi.org/10.1002/hlca.19860690824>
- Y. Kuramochi, O. Ishitani, H. Ishida, *Coord. Chem. Rev.* **2018**, *373*, 333. <https://doi.org/10.1016/j.ccr.2017.11.023>
- Y. Tamaki, O. Ishitani, *ACS Catal.* **2017**, *7*, 3394. <https://doi.org/10.1021/acscatal.7b00440>
- A. J. Morris, G. J. Meyer, E. Fujita, *Acc. Chem. Res.* **2009**, *42*, 1983. <https://doi.org/10.1021/ar9001679>
- K. E. Dalle, J. Warnan, J. J. Leung, B. Reuillard, I. S. Karmel, E. Reisner, *Chem. Rev.* **2019**, *119*, 2752. <https://doi.org/10.1021/acs.chemrev.8b00392>
- S. Yoshino, T. Takayama, Y. Yamaguchi, A. Iwase, A. Kudo, *Acc. Chem. Res.* **2022**, *55*, 966. <https://doi.org/10.1021/acs.accounts.1c00676>
- A. Nakada, H. Kumagai, M. Robert, O. Ishitani, K. Maeda, *Acc. Mater. Res.* **2021**, *2*, 458. <https://doi.org/10.1021/accountsmr.1c00060>
- H. Kumagai, Y. Tamaki, O. Ishitani, *Acc. Chem. Res.* **2022**, *55*, 978. <https://doi.org/10.1021/acs.accounts.1c00705>

9. T. Morikawa, S. Sato, K. Sekizawa, T. M. Suzuki, T. Arai, *Acc. Chem. Res.* **2022**, *55*, 933. <https://doi.org/10.1021/acs.accounts.1c00564>
10. J. Eppinger, K.-W. Huang, *ACS Energy Lett.* **2017**, *2*, 188. <https://doi.org/10.1021/acsenergylett.6b00574>
11. J. F. Hull, Y. Himeda, W.-H. Wang, B. Hashiguchi, R. Periana, D. J. Szalda, J. T. Muckerman, E. Fujita, *Nat. Chem.* **2012**, *4*, 383. <https://doi.org/10.1038/nchem.1295>
12. N. Onishi, M. Iguchi, X. Yang, R. Kanega, H. Kawanami, Q. Xu, Y. Himeda, *Adv. Energy Mater.* **2019**, *9*, 1801275. <https://doi.org/10.1002/aenm.201801275>
13. K. Sekizawa, K. Maeda, K. Domen, K. Koike, O. Ishitani, *J. Am. Chem. Soc.* **2013**, *135*, 4596. <https://doi.org/10.1021/ja311541a>
14. R. Kuriki, H. Matsunaga, T. Nakashima, K. Wada, A. Yamakata, O. Ishitani, K. Maeda, *J. Am. Chem. Soc.* **2016**, *138*, 5159. <https://doi.org/10.1021/jacs.6b01997>
15. R. Kuriki, M. Yamamoto, K. Higuchi, Y. Yamamoto, M. Akatsuka, D. Lu, S. Yagi, T. Yoshida, O. Ishitani, K. Maeda, *Angew. Chem. Int. Ed.* **2017**, *56*, 4867. <https://doi.org/10.1002/anie.201701627>
16. N. Sakakibara, M. Shizuno, T. Kanazawa, K. Kato, A. Yamakata, S. Nozawa, T. Ito, K. Terashima, K. Maeda, Y. Tamaki, O. Ishitani, *ACS Appl. Mater. Interfaces* **2023**, *15*, 13205. <https://doi.org/10.1021/acsami.3c00955>
17. Y. Tamaki, K. Koike, O. Ishitani, *Chem. Sci.* **2015**, *6*, 7213. <https://doi.org/10.1039/C5SC02018B>
18. Y. Tamaki, T. Morimoto, K. Koike, O. Ishitani, *PNAS* **2012**, *109*, 15673. <https://doi.org/10.1073/pnas.1118336109>
19. J. Kosco, F. Moruzzi, B. Willner, I. McCulloch, *Adv. Energy Mater.* **2020**, *10*, 2001935. <https://doi.org/10.1002/aenm.202001935>
20. C. M. Aitchison, R. S. Sprick, *Nanoscale* **2021**, *13*, 634. <https://doi.org/10.1039/D0NR07533G>
21. R. S. Sprick, J. X. Jiang, B. Bonillo, S. Ren, T. Ratvijitvech, P. Guiglion, M. A. Zwijnenburg, D. J. Adams, A. I. Cooper, *J. Am. Chem. Soc.* **2015**, *137*, 3265. <https://doi.org/10.1021/ja511552k>
22. S. A. J. Hillman, R. S. Sprick, D. Pearce, D. J. Woods, W.-Y. Sit, X. Shi, A. I. Cooper, J. R. Durrant, J. Nelson, *J. Am. Chem. Soc.* **2022**, *144*, 19382. <https://doi.org/10.1021/jacs.2c07103>
23. M. Sachs, R. S. Sprick, D. Pearce, S. A. J. Hillman, A. Monti, A. A. Y. Guilbert, N. J. Brownbill, S. Dimitrov, X. Shi, F. Blanc, M. A. Zwijnenburg, J. Nelson, J. R. Durrant, A. I. Cooper, *Nat. Commun.* **2018**, *9*, 4968. <https://doi.org/10.1038/s41467-018-07420-6>
24. E. McQueen, N. Sakakibara, K. Kamogawa, M. A. Zwijnenburg, Y. Tamaki, O. Ishitani, R. S. Sprick, *Chem. Sci.* **2024**, *15*, 18146. <https://doi.org/10.1039/D4SC05289G>
25. R. S. Sprick, B. Bonillo, R. Clowes, P. Guiglion, N. J. Brownbill, B. J. Slater, F. Blanc, M. A. Zwijnenburg, D. J. Adams, A. I. Cooper, *Angew. Chem. Int. Ed.* **2016**, *128*, 1824. <https://doi.org/10.1002/ange.201510542>
26. Y. Bai, C. Li, L. Liu, Y. Yamaguchi, M. Bahri, H. Yang, A. Gardner, M. A. Zwijnenburg, N. D. Browning, A. J. Cowan, A. Kudo, A. I. Cooper, R. S. Sprick, *Angew. Chem. Int. Ed.* **2022**, *61*, e202201299. <https://doi.org/10.1002/anie.202201299>
27. F. Arcudi, L. Đorđević, B. Nagasing, S. I. Stupp, E. A. Weiss, *J. Am. Chem. Soc.* **2021**, *143*, 18131. <https://doi.org/10.1021/jacs.1c06961>
28. D. Kim, S. Bhattacharjee, E. Lam, C. Casadevall, S. Rodríguez-Jiménez, E. Reisner, *Small* **2024**, *20*, 2400057. <https://doi.org/10.1002/smll.202400057>
29. K. Ishihara, A. Nakada, H. Suzuki, O. Tomita, S. Nozawa, A. Saeki, R. Abe, *J. Mater. Chem. A* **2024**, *12*, 30279. <https://doi.org/10.1039/D4TA04014G>
30. B. Cai, M. Axelsson, S. Zhan, M. V. Pavliuk, S. Wang, J. Li, H. Tian, *Angew. Chem. Int. Ed.* **2023**, *62*, e202312276. <https://doi.org/10.1002/anie.202312276>
31. Y.-C. Hao, L.-W. Chen, J. Li, Y. Guo, X. Su, M. Shu, Q. Zhang, W.-Y. Gao, S. Li, Z.-L. Yu, L. Gu, X. Feng, A.-X. Yin, R. Si, Y.-W. Zhang, B. Wang, C.-H. Yan, *Nat. Commun.* **2021**, *12*, 2682. <https://doi.org/10.1038/s41467-021-22991-7>
32. C. D. Sahn, G. M. Ucoski, S. Roy, E. Reisner, *ACS Catal.* **2021**, *11*, 11266. <https://doi.org/10.1021/acscatal.1c02921>
33. M. F. Kuehnel, C. D. Sahn, G. Neri, J. R. Lee, K. L. Orchard, A. J. Cowan, E. Reisner, *Chem. Sci.* **2018**, *9*, 2501. <https://doi.org/10.1039/C7SC04429A>
34. M. F. Kuehnel, K. L. Orchard, K. E. Dalle, E. Reisner, *J. Am. Chem. Soc.* **2017**, *139*, 7217. <https://doi.org/10.1021/jacs.7b00369>
35. X. Zhang, K. Yamauchi, K. Sakai, *ACS Catal.* **2021**, *11*, 10436. <https://doi.org/10.1021/acscatal.1c02475>
36. A. Nakada, K. Koike, T. Nakashima, T. Morimoto, O. Ishitani, *Inorg. Chem.* **2015**, *54*, 1800. <https://doi.org/10.1021/ic502707t>
37. A. Nakada, T. Nakashima, K. Sekizawa, K. Maeda, O. Ishitani, *Chem. Sci.* **2016**, *7*, 4364. <https://doi.org/10.1039/C6SC00586A>
38. A. Nakada, R. Kuriki, K. Sekizawa, S. Nishioka, J. J. M. Vequizo, T. Uchiyama, N. Kawakami, D. Lu, A. Yamakata, Y. Uchimoto, O. Ishitani, K. Maeda, *ACS Catal.* **2018**, *8*, 9744. <https://doi.org/10.1021/acscatal.8b03062>
39. J.-S. Lee, D.-I. Won, W.-J. Jung, H.-J. Son, C. Pac, S. O. Kang, *Angew. Chem. Int. Ed.* **2017**, *56*, 976. <https://doi.org/10.1002/anie.201608593>
40. T. W. Woolerton, S. Sheard, E. Reisner, E. Pierce, S. W. Ragsdale, F. A. Armstrong, *J. Am. Chem. Soc.* **2010**, *132*, 2132. <https://doi.org/10.1021/ja910091z>
41. S. Takizawa, T. Okuyama, S. Yamazaki, K. Sato, H. Masai, T. Iwai, S. Murata, J. Terao, *J. Am. Chem. Soc.* **2023**, *145*, 15049. <https://doi.org/10.1021/jacs.3c03625>
42. N. Ikuta, S. Takizawa, S. Murata, *Photochem. Photobiol. Sci.* **2014**, *13*, 691. <https://doi.org/10.1039/c3pp50429h>
43. Y. Kuramochi, J. Itabashi, K. Fukaya, A. Enomoto, M. Yoshida, H. Ishida, *Chem. Sci.* **2015**, *6*, 3063. <https://doi.org/10.1039/C5SC00199D>
44. Y. Kuramochi, M. Kamiya, H. Ishida, *Inorg. Chem.* **2014**, *53*, 3326. <https://doi.org/10.1021/ic500050q>
45. S. Yoshino, A. Iwase, Y. Yamaguchi, T. M. Suzuki, T. Morikawa, A. Kudo, *J. Am. Chem. Soc.* **2022**, *144*, 2323. <https://doi.org/10.1021/jacs.1c12636>
46. C. M. Aitchison, M. Sachs, M. A. Little, L. Wilbraham, N. J. Brownbill, C. M. Kane, F. Blanc, M. A. Zwijnenburg, J. R. Durrant, R. S. Sprick, A. I. Cooper, *Chem. Sci.* **2020**, *11*, 8744. <https://doi.org/10.1039/D0SC02675A>
47. M. Sachs, H. Cha, J. Kosco, C. M. Aitchison, L. Francàs, S. Corby, C.-L. Chiang, A. A. Wilson, R. Godin, A. Fahey-Williams, A. I. Cooper, R. S. Sprick, I. McCulloch, J. R. Durrant, *J. Am. Chem. Soc.* **2020**, *142*, 14574. <https://doi.org/10.1021/jacs.0c06104>
48. J. Kosco, I. McCulloch, *ACS Energy Lett.* **2018**, *3*, 2846. <https://doi.org/10.1021/acsenergylett.8b01853>
49. J. Kosco, M. Sachs, R. Godin, M. Kirkus, L. Francas, M. Bidwell, M. Qureshi, D. Anjum, J. R. Durrant, I. McCulloch, *Adv. Energy Mater.* **2018**, *8*, 1802181. <https://doi.org/10.1002/aenm.201802181>
50. P. A. Anderson, G. B. Deacon, K. H. Haarmann, F. R. Keene, T. J. Meyer, D. A. Reitsma, B. W. Skelton, G. F. Strouse, N. C. Thomas, *Inorg. Chem.* **1995**, *34*, 6145. <https://doi.org/10.1021/ic00128a028>
51. K. Maeda, R. Kuriki, M. Zhang, X. Wang, O. Ishitani, *J. Mater. Chem. A* **2014**, *2*, 15146. <https://doi.org/10.1039/C4TA03128H>
52. N. Sakakibara, K. Kamogawa, A. Miyoshi, K. Maeda, O. Ishitani, *Energy Fuels* **2024**, *38*, 2343. <https://doi.org/10.1021/acs.energyfuels.3c04126>

53. Y. Pellegrin, F. Odobel, *C. R. Chim.* **2017**, *20*, 283. <https://doi.org/10.1016/j.crci.2015.11.026>
54. R. N. Sampaio, D. C. Grills, D. E. Polyansky, D. J. Szalda, E. Fujita, *J. Am. Chem. Soc.* **2020**, *142*, 2413. <https://doi.org/10.1021/jacs.9b11897>
55. Y. Yang, M. A. Zwijnenburg, A. M. Gardner, S. Adamczyk, J. Yang, Y. Sun, Q. Jiang, A. J. Cowan, R. S. Sprick, L.-N. Liu, A. I. Cooper, *ACS Nano* **2024**, *18*, 13484. <https://doi.org/10.1021/acsnano.3c10668>
56. Y. Yamazaki, H. Takeda, O. Ishitani, *J. Photochem. Photobiol. C* **2015**, *25*, 106. <https://doi.org/10.1016/j.jphotochemrev.2015.09.001>
57. Z. Fu, A. Vogel, M. A. Zwijnenburg, A. I. Cooper, R. S. Sprick, *J. Mater. Chem. A* **2021**, *9*, 4291. <https://doi.org/10.1039/D0TA09613J>
58. L. A. Frolova, N. P. Piven, D. K. Susarova, A. V. Akkuratov, S. D. Babenko, P. A. Troshin, *Chem. Commun.* **2015**, *51*, 2242. <https://doi.org/10.1039/C4CC08146C>
59. M. Tabbal, T. Christidis, S. Isber, P. Mérel, M. A. El Khakani, M. Chaker, A. Amassian, L. Martinu, *J. Appl. Phys.* **2005**, *98*, 044310. <https://doi.org/10.1063/1.2009817>
60. P. Stathi, L. Belles, Y. Deligiannakis, *J. Phys. Chem. C* **2022**, *126*, 14125. <https://doi.org/10.1021/acs.jpcc.2c02687>
61. T. Teranishi, H. Hori, M. Miyake, *J. Phys. Chem. B* **1997**, *101*, 5774. <https://doi.org/10.1021/jp970599y>